

Towards Top-Down Stereoscopic Image Quality Assessment via Stereo Attention

Huilin Zhang, Sumei Li, *Member, IEEE*, Yongli Chang

Abstract—Stereoscopic image quality assessment (SIQA) plays a crucial role in evaluating and improving the visual experience of 3D content. Existing binocular properties and attention-based methods for SIQA have achieved promising performance. However, these bottom-up approaches are inadequate in exploiting the inherent characteristics of the human visual system (HVS). This paper presents a novel network for SIQA via stereo attention, employing a top-down perspective to guide the quality assessment process. Our proposed method realizes the guidance from high-level binocular signals down to low-level monocular signals, while the binocular and monocular information can be calibrated progressively throughout the processing pipeline. We design a generalized Stereo Attention (SAT) block to implement the top-down philosophy in stereo perception. This block utilizes the fusion-generated attention map as a high-level binocular modulator, influencing the representation of two low-level monocular features. Additionally, we introduce an Energy Coefficient (EC) to account for recent findings indicating that binocular responses in the primate primary visual cortex are less than the sum of monocular responses. The adaptive EC can tune the magnitude of binocular response flexibly, thus enhancing the formation of robust binocular features within our framework. To extract the most discriminative quality information from the summation and subtraction of the two branches of monocular features, we utilize a dual-pooling strategy that applies min-pooling and max-pooling operations to the respective branches. Experimental results highlight the superiority of our top-down method in simulating the property of visual perception and advancing the state-of-the-art in the SIQA field. The code of this work is available at <http://github.com/>.

Index Terms—Stereoscopic image quality assessment, Top-Down, Stereo Attention, Human Visual System, Binocular Characteristics.

I. INTRODUCTION

WE have seen a lot of 3D-related multimedia products launched over the past decade. Toward creating a more immersive stereo world, stereoscopic information processing technologies attract attention from both industry and academia. Since stereo images degrade inevitably during the acquisition, processing, and transmission, stereoscopic image quality assessment (SIQA) has become the first imperative. In view of pristine images barely obtained in practical applications, no-reference SIQA (NR-SIQA) is exactly our focus.

Considering that the quality of a stereo image is evaluated by the human subjective perception in actual assessment, it is crucial to develop algorithms to mimic the human visual system (HVS) for effective NR-SIQA. Numerous previous studies in the literature provided deep insights into HVS. Specifically, universal HVS characteristics include binocular properties (binocular fusion and rivalry) [1], hierarchical interaction [2], cognitive reasoning mechanisms (bottom-up and

top-down) [3], [4], etc. In effect, earlier NR-SIQA methods have explored in implementing HVS through traditional algorithms since the significance of HVS characteristics. However, these works [5]–[9] highly depend on hand-crafted features and are not robust and generalizable enough to represent inherent properties in stereo images. In the past few years, we have witnessed both the prosperity of convolutional neural networks (CNN) and self-attention algorithms in the computer vision community. CNN and attention module both reflect the philosophy of HVS since their design is inspired by the signal-processing and attention mechanism of neurons in the human brain, respectively. Especially, CNN has become a landmark in NR-SIQA, as well as other computer vision tasks like image classification [10], semantic segmentation [11], and object detection [12].

Currently, CNN-based methods have been the mainstream approaches in the NR-SIQA field since these methods would predict the quality of a stereo image more precisely due to their ability to mimic human perceptual characteristics. For example, Zhang et al. [13] first introduced CNN into the NR-SIQA field, proposing a three-column CNN model with the left view, right view, and their difference map as inputs. Extracted high-level features from three branches are finally concatenated to feed into a Multi-Layer Perception (MLP), obtaining the quality score. Fang et al. [14] proposed a Siamese network in which two branches of the network share the same weights. Feature maps from two monocular branches as the outputs of the Siamese network are concatenated before the final regression of the quality score. Shi et al. [15] designed an RM-CNN3 model, employing a similar philosophy with [13], while their network focuses on multi-task SIQA. Although these works have achieved promising quality evaluation performance by utilizing the advantages of CNN architecture, they do not take complex binocular properties into account. The interaction between binocular and monocular features is lacked or implicitly used in these literature, which is naïve and inadequate.

With diving deeper into HVS, more works have begun to mimic hierarchical interaction in their research. Zhou et al. [16] designed a dual-stream network with binocular interaction in multiple layers, and they concatenated fusion and difference maps that are regarded as interactive information. Bourbia et al. [17] employed and modified [16]’s model, leveraging naturalness analysis to develop a multi-task CNN for SIQA. Both [16] and [17] use multi-level difference and fusion features to facilitate the model’s performance. A multi-level feature fusion network was proposed in [18], where three types of features extracted from three different levels were

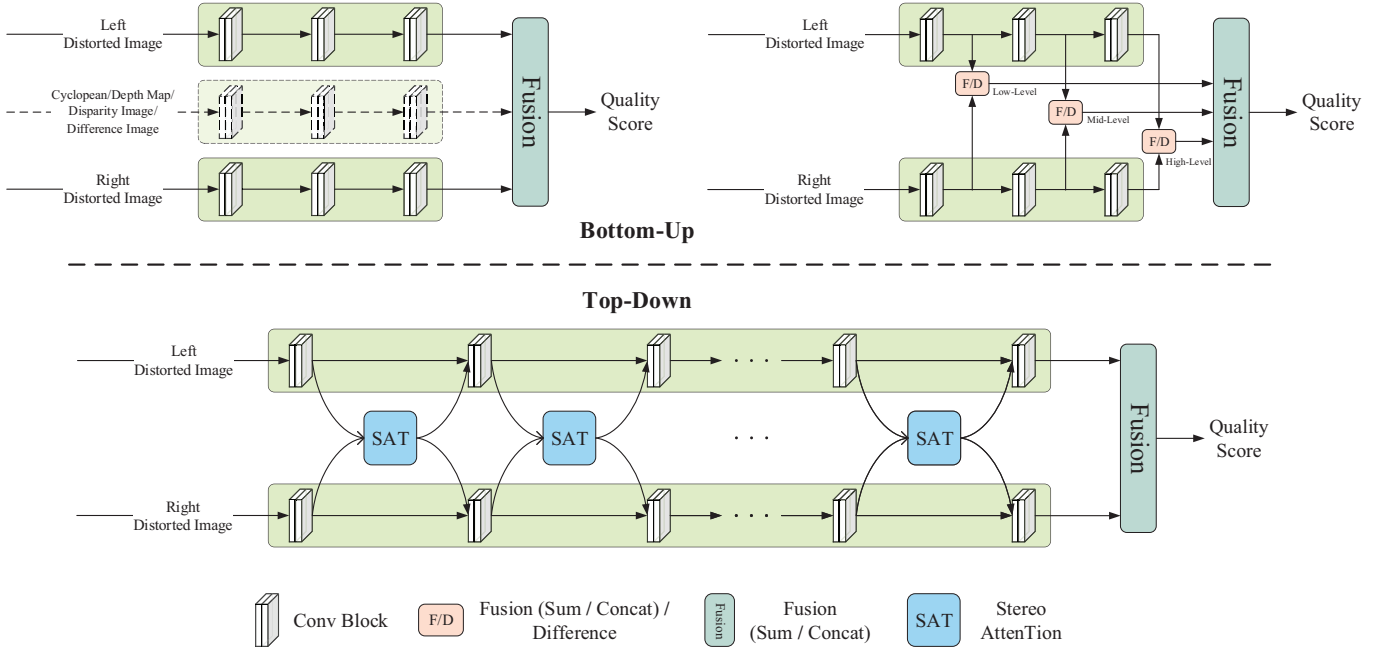


Fig. 1. Intuitive comparison between general bottom-up methods and our top-down method for NR-SIQA.

concatenated and regressed as quality output. These networks with multiple interactions during the processing have gained better results, which proves the significance of binocular characteristics in SIQA.

From the network design perspective, the above-mentioned methods [13]–[18] can be categorized into two types: 1) the processing of each view is wholly separated, without any (explicitly) interaction [13]–[15]. 2) hierarchical features are extracted through the pipeline, and the fusion or difference features are obtained as the interactive information for further transmission [16]–[18]. As depicted in the upper left part of Fig. 1, the first category only considers the monocular vision and ignores the binocular interaction mechanism of the HVS. The second category is simplified and illustrated in the upper right part of Fig. 1. These metrics have obtained good results due to the benefits of simulating binocular interactive phenomena. These SIQA models considering HVS properties share the same design philosophy, i.e., extracting preliminary monocular visual characteristics and processing them to form abstract binocular ones straightforward, then regressing obtained binocular features to get the overall quality estimation. Such a kind of design philosophy can be considered a bottom-up strategy. We claim that this design philosophy has some inherent drawbacks. First, the interactions among binocular and monocular signals are difficult to be characterized. Second, without guidance from high-level binocular signals down to low-level monocular ones, it is hard to adapt to quality-aware tasks. Therefore, the performance of the existing SIQA models remains limited.

Moreover, as plug-and-play modules, it is a common practice to insert self-attention modules sequentially with convolution blocks in a CNN-based architecture, which realizes the recalibration of the feature responses of a single input. When it comes to stereo pairs, we naturally raise a question:

is the attention mechanism appropriate to cope with stereo vision like SIQA? Researchers have made some explorations. Zhou et al. [19] used attention modules after the left and right fusion implementation, and Li et al. [20] inserted a dual attention block following the feature extraction from Cyclopean image patches. Both of them reflect binocular characteristics implicitly via exploring inner relationships in combined features of two monocular views. Yet, their attempts to insert limited attention modules do not exploit the full potential of attention modules and are still bottom-up.

In the field of cognitive psychology and neuroscience, there are two types of reasoning mechanisms termed bottom-up and top-down strategy, respectively. Bottom-up reasoning implies the flow of information from lower-level, such as primary visual stimuli, up to higher-level perceptual procedures. In contrast, top-down processing refers to the opposite direction of information flow, where the higher-level cognitive processes could be expectations and prior knowledge [4]. In the IQA context, people’s task is to distinguish the perceptual quality distortion and give a quality score of degraded image. This task is high-level and different from other vision tasks because quality-related expectations, such as distorted types and degrees, would influence how we perceive and assess the quality of an image. Literature [3] pointed out that the top-down mechanism operates through a continuous feedback loop with bottom-up processes, i.e., the feedback from higher-level processes can modulate and refine the early sensory representations, enhancing or suppressing certain features based on contextual information and expectations. Therefore, we intuitively come up with the idea to implement the top-down process by constructing a Stereo Attention structure, employing an attention map as the higher-level binocular guidance to monocular signals since it can reflect the expectations of human’s most interests and is relatively advanced compared to

the input of the attention module. We also stack SAT blocks to realize a consecutive feedback loop. Thus, the architecture of a top-down Stereo Attention Network (SATNet) is established. Two above-mentioned general bottom-up manners and our top-down pipeline are compared intuitively in Fig. 1.

Furthermore, we introduce an Energy Coefficient (EC) and a dual-pooling strategy into our model to make SATNet more sensible and well-performing. Recently, biological researchers have put forward that binocular responses in primate primary visual cortex are less than the sum of monocular responses of two eyes in their earlier report [21]. Zhang et al. [22] proved this fact by investigating neuronal responses in macaque V1 with two-photon calcium imaging. Whereas to the best of our knowledge, almost all previous works took all portions of two monocular responses into account, which is unreasonable to some extent. Thus, we introduce an EC into SAT structure to adaptively learn suitable binocular response magnitudes. In the classification and detection domain, max-pooling is often employed following feature encoding to reduce computational overhead, as well as maintain local structure invariance so as to facilitate object recognition. However, for the IQA task, good features should be able to capture quality properties such as noise and blur, which are normally the smaller values in the feature map. Toward adding quality-sensitive attributes to our model, we employ min-pooling while retaining max-pooling, named dual-pooling. We demonstrate the validity of our proposed dual-pooling strategy through empirical evaluation, showcasing its effectiveness in screening the most crucial structure and distortion information for quality regression.

Overall, the contributions of this work are three-fold:

- 1) We propose a stereo attention network for stereoscopic image quality assessment from a top-down perspective, which realizes the guidance from high-level binocular signals down to low-level monocular signals, while both the binocular and monocular information can be calibrated progressively throughout the processing pipeline.
- 2) We design a generalized Stereo Attention (SAT) block to implement the top-down philosophy in stereo image quality perception, where the attention map is leveraged as the high-level binocular modulator of two low-level monocular features. Moreover, an Energy Coefficient is introduced for binocular feature formation, reflecting the latest finding that binocular responses in the primate primary visual cortex are less than the sum of monocular responses.
- 3) To screen the most discriminative quality information from the summation and subtraction of the two branches of monocular features, we apply min-pooling and max-pooling to them, respectively, namely the dual-pooling strategy. Empirical evidence verifies the superiority of our strategy.

The remainder of this paper is organized as follows. In Section II, a review of related work is given. In Section III, we introduce the architecture and details of the proposed SATNet. Experimental results and analysis are given and discussed in Section IV. In addition, Section IV also gives the cross-dataset validation and ablation experiments. Finally, conclusions are

drawn in Section V.

II. RELATED WORK

A. NR-SIQA Methods

Eminent NR-SIQA methods have evolved through two phases. In the early stage, pioneers generally extract hand-crafted features from stereo pairs and regress them to quality scores by different machine learning tools. With the bloom of CNN, researchers have developed substantial CNN-based SIQA models focusing on integrating feature extraction and quality regression in an end-to-end way. Therefore, in this subsection, we review conventional and CNN-based NR-SIQA methods respectively.

For traditional methods, researchers usually extract features, including Natural Scene Statistics (NSS) and HVS, manually. Then they employ ordinary machine learning models, e.g., Support Vector Regression (SVR), K-Nearest Neighbors (KNN), Extreme Learning Machine (ELM), etc., to integrate these artificial features into predicted quality scores. For instance, Chen et al. [23] developed a blind IQA model for stereo images, in which NSS features are used to train a support vector machine model to predict the quality. Yang et al. devised a model for NR-SIQA in [24], employing deep belief network (DBN) and SVR to regress NSS features. Similar to [24], an effective blind metric evaluating stereo images via DBN is proposed in [25], where local histogram of oriented gradient (HoG) features from high-frequency wavelet coefficients and global statistical features including magnitude, variance, and entropy are extracted. Three DBNs are used for mapping these NSS features to quality scores. These mentioned approaches are highly dependent on natural statistical characteristics of distorted stereo images, which do not take human visual properties into account, thus resulting in limited performance. Different from those NSS-based IQA methods, some literature [5]–[9] extract features to represent HVS characteristics directly, then the machine learning tools are employed to train the quality prediction model. For example, Zhou and Yu developed a binocular response-based NR-SIQA method in [5]. Binocular responses, including Binocular Energy Response (BER) and Binocular Rivalry Response (BRR) of stereo pairs, can be obtained. Furthermore, the final quality score can be derived from produced quality-predictive features by KNN. An NR-SIQA model based on the binocular combination and ELM was devised by Zhou et al. [6]. Two binocular combinations of stimuli are generated via different strategies, then diverse binocular quality-aware features of the combinations are extracted by local binary pattern operators. Finally, an ELM is adopted to map obtained features to objective quality prediction. Fang et al. [7] proposed a no-reference quality evaluator of stereo pairs, getting monocular and binocular visual properties from left and right images. Further, they employed SVR to gain the final results. Liu et al. [8] designed a 3D image quality evaluator accounting for human monocular visual properties and binocular interactions. They modeled both monocular and binocular information and utilized an SVR to combine these features and assess the quality. Messai et al. [9] proposed an NR-SIQA network using

a neural network Adaptive Boosting (AdaBoost). Cyclopean views of distorted left and right images can be acquired to extract features including gradient magnitude, relative gradient magnitude, and gradient orientation. Then AdaBoost is employed to generate the final results.

These traditional works [5]–[9], [23]–[25] mainly include two steps: feature extraction and model training. In general, explicitly modeling variable visibility factors (e.g., color, luminance, intensity, structure, and depth) artificially and then regressing them to derive an overall quality estimation is an implementation of the bottom-up philosophy. In that case, there exist intrinsic disadvantages of hand-crafted features, such as complexity and imprecision, which may lead to performance deterioration. Accordingly, conventional NR-SIQA methods can not achieve high consistency with subjective assessment.

In the past decade, CNN has significantly boosted multiple computer vision tasks, of course, NR-SIQA involved. As we concluded in Section I, ordinary CNN-based methods can be categorized into two types. For the first category, the processing of each view is separated without any (explicit) interaction. Zhang et al. [13] took the first step in using CNN to estimate the quality of stereo pairs. Their pioneering work established a three-column CNN model and represented depth information with difference images. Extracted high-level features from the left view, right view, and difference map are simply concatenated before regression. Fang et al. [14] proposed a Siamese network to learn high-level monocular semantic information, then the outputs of two sharing-weights branches are concatenated to produce the final quality score. Shi et al. [15] built an RM-CNN3 model for multi-task SIQA, sharing a similar philosophy with [13]. Attributed to the interactive information between binocular and monocular features are lacking or implicitly used, these primary methods [13]–[15] cannot get the desirable evaluative capability. For the metrics belonging to the second category, they extract hierarchical features through the pipeline and conduct fusion and difference operations to obtain the interactive information for further transmission. Zhou et al. [16] devised a dual-stream network with multiple binocular interactions, and they utilized concatenation to fuse monocular features, fusion maps, and difference maps learned from different levels. Bourbia et al. [17] designed their multitask CNN for SIQA likewise, and multi-level difference and fusion features are exploited to facilitate the model’s performance. A multi-level feature fusion network was proposed in [18], where three types of features extracted from three different levels were concatenated and regressed as quality output. These works have strongly proved the significance of implementing binocular interactive properties in SIQA. Thereby, in recent years, researchers have designed more complex networks to mimic human visual perception and pursue better results. Shen et al. [26] conducted a cross-fusion strategy after primary feature extraction to model the fusion of left and right views occurring in the V1 cortex. Aiming to handle asymmetric distortion assessment, Messai et al. [27] proposed a deep multi-score model for NR-SIQA. The multi-score CNN incorporates left, right, and stereoscopic objective scores to extract the corresponding properties of each

view. Sim et al. [28] pointed out that evaluating perceptual quality and understanding semantics cannot be thoroughly separated, so they proposed a blind SIQA method based on binocular semantic and quality channels. Considering both binocular interaction and fusion mechanisms of the HVS, a hierarchical StereoIF-Net [29] for NR-SIQA is proposed to simulate the whole quality perception of 3D visual signals in the human cortex. Benefiting from that, StereoIF-Net has made advancements in evaluation results.

Although these CNN-based methods have reaped increasing performance through sophisticated model design, they are still bottom-up, i.e., visual signals are gradually integrated and processed from local details to global conception by the visual brain cortex. Unlike current mainstream approaches, our method models binocular interaction from a top-down perspective in an SAT-based fashion, which is more in line with the fact that visual cognition begins in the higher visual cortex and information is integrated with the lower counterpart.

B. Attention Mechanism.

The attention mechanism in computer vision aims to imitate the attention mechanism of human vision. To some extent, the attention mechanism is similar to the saliency theory, aiming to allocate more computational resources toward the most informative signal components. Attention has recently been extensively explored to facilitate various vision tasks. SENet [30] exploits channel interdependencies to re-weight the output of convolution blocks. Both channel and spatial relationships are taken into account in CBAM [31] to realize channel-wise and spatial-wise recalibration. In NLNet [32] and GCNet [33], self-attention is introduced to investigate long-range dependencies through non-local operations. SKNet [34] utilizes self-attention for kernel size selection.

However, few researchers pay attention to designing a particular attention module for stereo tasks. When it comes to the SIQA task, former researchers just inserted plain attention modules into their CNN architecture to boost performance. For instance, Zhou et al. [19] used a SE block followed after the fusion operation in three scales of the receptive field to reflect the competitive characteristic of binocular fusion implicitly. Li et al. [20] inserted a dual attention block following the feature extraction from Cyclopean image patches, accounting for both channel and spatial attention. Both of them transferred existing attention blocks into the SIQA context without any modification, trying to explore inner relationships in combined features of two monocular views and reflect binocular properties. Yet, their attempts to insert limited attention modules do not exploit the full potential of the attention mechanism and are still bottom-up. Compared to them, we modify old attention blocks to novel ones. Specifically, we introduce an EC and leverage a fusion-generated attention map, making our SAT block more suitable to implement top-down perception for the SIQA scenario. More details can be found in Section III-C.

III. PROPOSED METHOD

A. Network Architecture

Our proposed SATNet is an end-to-end CNN, it takes left and right image patches sized 40×40 as dual-channel inputs

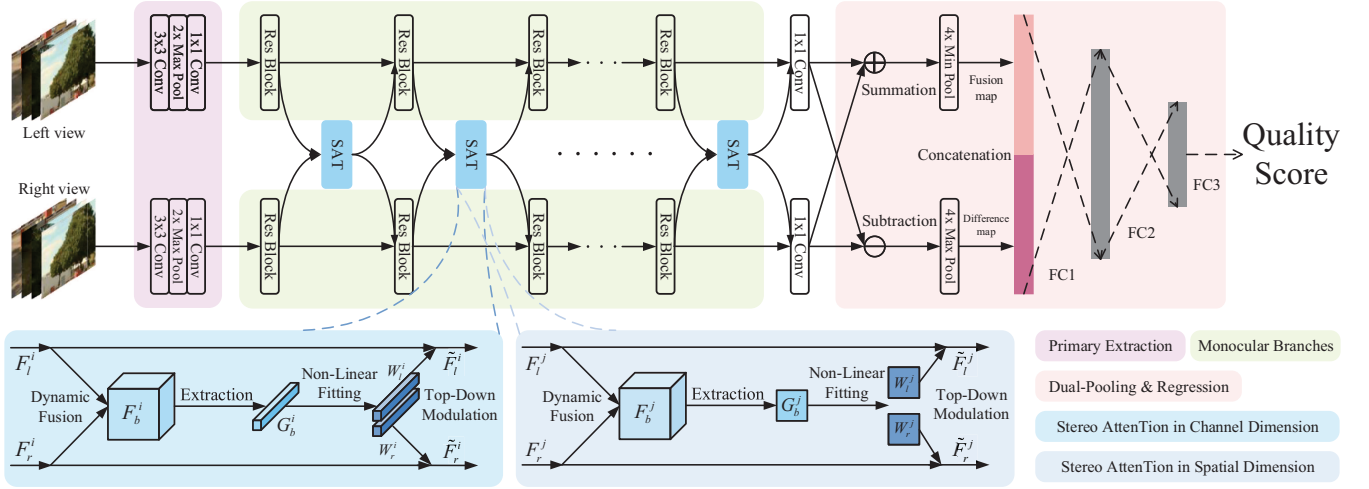


Fig. 2. The architecture of the proposed SATNet. Individual modules are termed in the corresponding color boxes in the lower right corner. In light that diverse attention modules focus on different attention dimensions, here we show two examples of SAT blocks in the channel and spatial dimensions.

and predicts a quality score as the final output. Fig. 2 shows the pipeline. SATNet consists of four main parts: Primary Extraction, two monocular branches, SAT blocks, and Dual-Pooling & Regression, their names are labeled in the corresponding color boxes in the lower right corner of Fig. 2.

First, stereo image patches are encoded in the Primary Extraction phase, in which two independent convolution layers sized 3×3 and 1×1 extract monocular features in left and right branches. Between two convolutions, a $2 \times$ max pooling layer exists, downsampling the feature maps to 20×20 pixels so subsequent layers could process signals more efficiently. We employ the most popular structure ResNet as the backbone of two monocular branches, leveraging its strong performance and efficiency in extracting features. The central part of SATNet is several chain-stacked res blocks, with each pair of res blocks followed by an SAT block. Given that our SAT blocks are transferred and modified from existing general attention modules, and diverse attention modules focus on different attention dimensions, here we show two examples of SAT blocks in the channel and spatial dimensions in the lower part of Fig. 2, respectively. After that, we use two convolution layers with 1×1 kernel size again to decode the outputs of two monocular branches separately. Next, as Fig. 2 depicts, a Dual-Pooling & Regression module is constructed. We perform summation and subtraction operations on two monocular features to generate fusion and difference maps, respectively. It is worth noting that all operations prior do not change the resolution of feature maps. Afterward, obtained fusion maps are $4 \times$ min-pooled, while the difference maps are $4 \times$ max-pooled. Finally, fusion and difference maps sized 5×5 are flattened and concatenated, then three fully connected (FC) layers regress them to a quality score. During the inference stage, the quality score of a complete stereo pair is calculated by averaging all scores of patches from it. The details of two monocular branches, SAT blocks, and Dual-Pooling & Regression are elaborated in the following subsections.

TABLE I
THE DETAILED CONFIGURATIONS OF PROPOSED SATNET.

Layer	Configuration <i>S/P/B^N/ReLU</i>	Input Dimension $C \times H \times W$	Output Dimension $C \times H \times W$
Primary Extraction	3×3 Conv	$1/1/\surd/\surd$	$3 \times 40 \times 40$
	$2 \times$ Max Pool	$2/-/-/-$	$64 \times 40 \times 40$
	1×1 Conv	$-/-/-/-$	$64 \times 20 \times 20$
Basic Block in Monocular Branches	3×3 Conv	$1/1/\surd/\surd$	$64 \times 20 \times 20$
	3×3 Conv	$1/1/\surd/\surd$	$64 \times 20 \times 20$
Bottleneck Block in Monocular Branches	1×1 Conv	$-/-/\surd/\surd$	$64 \times 20 \times 20$
	3×3 Conv	$1/1/\surd/\surd$	$64 \times 20 \times 20$
	1×1 Conv	$-/-/\surd/\surd$	$64 \times 20 \times 20$
Stereo Attention			$64 \times 20 \times 20$
	1×1 Conv	$-/-/-/-$	$64 \times 20 \times 20$
Dual-Pooling & Regression	$4 \times$ Min Pool	$4/-/-/-$	$64 \times 20 \times 20$
	$4 \times$ Max Pool	$4/-/-/-$	$64 \times 20 \times 20$
	FC1	$-/-/-/\surd$	3200
	FC2	$-/-/-/\surd$	1600
	FC3	$-/-/-/\surd$	800
			1

^S Stride
^P Padding
^{B^N} Batch Normalization
^{ReLU} ReLU activation function
 $C \times H \times W$ Channel \times Height \times Width
 $-$ indicates no corresponding parameter
 \surd indicates that BN/ReLU is equipped in the corresponding layer

B. Monocular Branches

He et al. [35] proposed the renowned ResNet of five different scales equipped with corresponding residual blocks. Specifically, shallow models (ResNet-18/34) are composed of basic blocks with two convolutional layers with 3×3 kernel size, and deeper networks (ResNet-50/101/152) are designed with bottleneck units considering the imperative of reducing computational overhead in the meantime of remaining model's depth. The bottleneck block includes two convolutional layers sized 1×1 and a convolutional layer with 3×3 kernel size in the middle. To enhance the learning ability of the feature representation and avoid the gradient vanishing problem, we adopt residual blocks to establish a dual-stream ResNet as the backbone of monocular branches. Different from the original residual blocks [35], we employ the better residual blocks with full pre-activation to boost performance, which benefits from enhanced identity mappings [36]. Two blocks are illustrated as Fig. 3.

In our design, the left and right res blocks of the same level

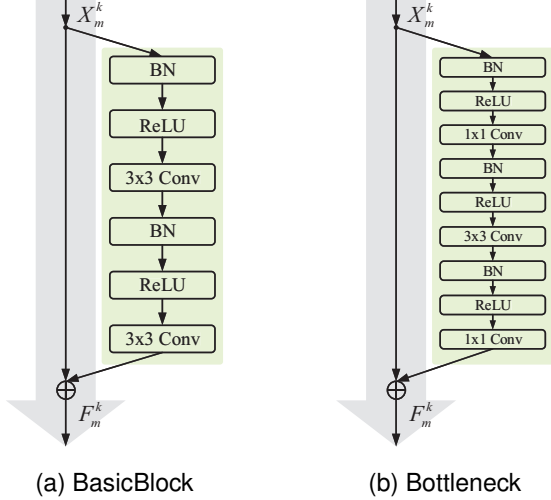


Fig. 3. Two variants of Res Block with full pre-activation.

are followed by an SAT block. So we construct our model with different scales with a range of SAT block numbers (K). Here we assign $K = 3, 7, 14, 15$, respectively, corresponding to four scales models (Depth = 11, 19, 33, 50, respectively). Referring to [35], we employ basic blocks to compose shallow models (Depth = 11, 19, 33) while building the deep model (50 layers) via bottleneck blocks, and the detailed configurations are listed in Table I. Let $X_m^k \in \mathbb{R}^{C \times H \times W}$ ($m \in \{l, r\}$, $k = 1, 2, \dots, K$) be the input feature of the k -th res block, the output $F_m^k \in \mathbb{R}^{C \times H \times W}$ can be described as

$$F_m^k = f_m(X_m^k, \omega_m^f), \quad (1)$$

where $f_m(\cdot, \omega_m^f)$ is the abstract res block function for monocular branch $m \in \{l, r\}$. The left and right branches do not share parameters and ω_m^f represents corresponding parameters.

C. Stereo Attention (SAT)

Attention modules are inborn to model binocular responses, benefiting from their information aggregation and non-linear abilities. Inspired by [32], [33], in which general attention module framework and components have been studied, we formulate SAT structure in three components: **Dynamic Fusion & Extraction**, **Non-Linear Fitting**, and **Top-Down Modulation**. These components are generic and not confined to a particular attention block [37]. Considering the diverse attention dimensions targeted by various attention modules, we present two instances of SAT blocks, one in the channel dimension ($k = i$) and the other in the spatial dimension ($k = j$), depicted in the lower section of Fig. 2. For building SATNet for the NR-SIQA task, we also exemplify three classic attention blocks (SE [30], CBAM [31], GC [33]) and their modeling by using our proposed structure. Details are shown in Fig. 4.

1) **Dynamic Fusion & Extraction**: It is designed to achieve two functions: Dynamically integrating features of two monocular branches, and further extracting critical information. Here we introduce an Energy Coefficient α to adaptively control the

magnitude of binocular fusion features F_b^k based on different inputs. Learnable α is constrained into $(0, 1)$ and multiplied by the summation of inputs of an SAT block F_l^k and F_r^k . We can write as

$$F_b^k = \alpha \times (F_l^k + F_r^k), \quad (2)$$

where “ \times ” denotes element-wise multiplication and “ $+$ ” indicates element-wise summation. α varies according to different factors, e.g., different SAT blocks, different phases (k), and different input features (F_l^k and F_r^k). Thus, during the inference stage, each response magnitude of the binocular fusion feature is regulated accurately by the corresponding EC, which is more consistent with the actual perception process and beneficial to boost network performance.

We define the feature extraction function after dynamic fusion as $g(\cdot, \omega^g)$, where ω^g is the parameter of the extractor g . Since pooling operation is often used for integration (i.e., SE, CBAM), g is usually a parameter-free operation (ω^g is not needed) and can be simplified as $g(\cdot)$. The flexibility of g makes obtained binocular feature G_b^k take different shapes depending on the extraction operation. We give some examples as follows:

$$G_b^k = \begin{cases} g(F_b^k), & \text{in SAT-SE, where } G_b^k \in \mathbb{R}^{C \times 1 \times 1} \\ g(F_b^k), & \text{spatial attention in SAT-CBAM,} \\ & \text{where } G_b^k \in \mathbb{R}^{2 \times H \times W} \\ g(F_b^k, \omega^g), & \text{in SAT-GC, where } G_b^k \in \mathbb{R}^{C \times 1 \times 1} \end{cases} \quad (3)$$

2) **Non-Linear Fitting**: This part generally transforms the gathered binocular features G_b^k into two high-level attention maps by using a series of FC layers and non-linear activations. Instead of an original sigmoid function (SE and CBAM), a softmax function is substituted to generate two sum-to-one weights W_l^k and W_r^k for two monocular branches. As for the attention module (GC) whose last layer was originally designed as FC, we assign the output dimension of FC as 2 to generate W_l^k and W_r^k . The derivation process can be described as

$$(W_l^k, W_r^k) = w(G_b^k, \omega^w), \quad W_l^k + W_r^k = 1, \quad (4)$$

where $w(\cdot, \omega^w)$ denotes the fitting function and ω^w is the used parameter.

3) **Top-Down Modulation**: In this component, previously generated high-level attention maps W_l^k and W_r^k are utilized as a binocular top-down modulation signal to guide the recalibration of two low-level monocular features F_l^k and F_r^k . The procedure of modulation is simple and convenient:

$$\tilde{F}_m^k = W_m^k \otimes F_m^k, \quad m \in \{l, r\}, \quad (5)$$

where \tilde{F}_m^k is the recalibrated monocular feature as well as the output of SAT block. “ \otimes ” represents the fusion operation. When the design is scaled dot-product attention, “ \otimes ” performs element-wise multiplication (SE and CBAM), and summation otherwise (GC).

It is worthwhile noting that during the inference stage, once the input stereo pairs change, α and W_m^k in different phases also change. Experiments results prove that it is especially effective to tackle asymmetric distortions, which further illustrates its inherent philosophy.

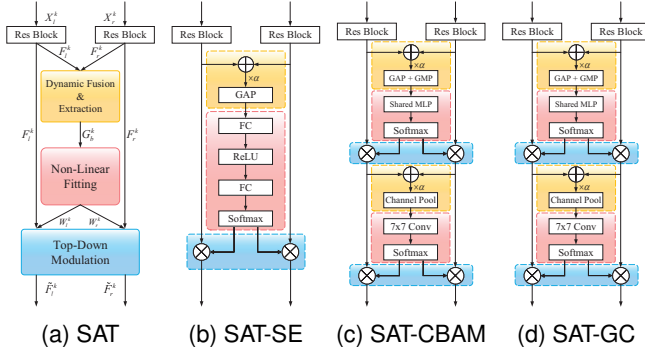


Fig. 4. We model a Stereo Attention (SAT) block with three components: Dynamic Fusion & Extraction, Non-Linear Fitting, and Top-Down Modulation. Here we show three instances of this structure: (b) SAT-SE, (c) SAT-CBAM, and (d) SAT-GC. “ \oplus ” denotes element-wise summation, “ \otimes ” represents element-wise multiplication, and “ \odot ” performs matrix multiplication.

D. Dual-Pooling & Regression

At the end of monocular branches and the last SAT block, a convolution layer with 1×1 kernel size is used to decode the outputs of them. Further, we process the two abstract monocular features.

As done in most NR-SIQA methods [8], [16], [17], [29], [38], we utilize summation and subtraction operations on two recalibrated high-level monocular features to get fusion and difference maps, which both contain much parallax information. We then apply dual-pooling on them to reduce parameters and screen the most crucial quality information for regression. Specifically, the fusion maps are $4 \times$ min-pooled, while the difference maps are $4 \times$ max-pooled. Finally, we flatten the obtained two 5×5 abstract quality features and concatenate them together. Three FC layers regress them to a predicted quality score of the stereo pair patches. Moreover, the first two FC layers are each followed by a ReLU function and a dropout unit [39] (dropout rate = 0.5), aiming to activate neurons and prevent overfitting.

IV. EXPERIMENTS AND RESULTS

A. Database

To evaluate the performance of the proposed method for NR-SIQA, we conducted our experiments on four public 3D databases: LIVE 3D Phase I [40], LIVE 3D Phase II [1], [23], WIVC 3D Phase I [41], and WIVC 3D Phase II [42]. A detailed introduction of four databases is given below:

1) *LIVE 3D Phase I*: This database contains five types of distortion: Gaussian Blur (Blur), Fast-Fading (FF), JPEG2000 (JP2K) compression, JPEG compression (JPEG), and Additive White Gaussian Noise (WN). The dataset consists of 20 reference images and 365 distorted images (80 pairs each for JPEG, JP2K, WN, FF, and 45 for Blur) with co-registered human scores in the form of Differential Mean Opinion Score (DMOS). All distortions are symmetric in nature. Depth maps and disparity maps are also provided for reference images.

2) *LIVE 3D Phase II*: 8 reference images and 360 distorted images with co-registered human scores in the form of DMOS are contained in this database. The distortion types are the

same as in LIVE 3D Phase I. For each distortion type, every reference stereo pair was processed to create 3 symmetric distorted stereo pairs and 6 asymmetric distorted stereo pairs. In total, there are 120 symmetrically and 240 asymmetrically distorted stereo images. Depth maps and disparity maps of reference images are also given.

3) *WIVC 3D Phase I*: This database provides 6 pristine stereo pairs and thus their corresponding single-view images, which are employed to generate distorted stereo pairs, either symmetrically or asymmetrically. Each single-view image is altered by three types of distortions (WN, Blur, and JPEG), and each distortion type has four distortion levels. Altogether, there are 324 distorted stereo images with their Mean Opinion Score (MOS).

4) *WIVC 3D Phase II*: The database is created from 10 pristine stereo image pairs. Like WIVC 3D Phase I database, each single-view image of the reference pair is processed by the same three distortion types and four distortion levels. Totally, there are 450 symmetric and asymmetric distorted stereo images with their co-registered MOS values.

B. Performance Index

In this paper, we employ three indicators including Pearson Linear Correlation Coefficient (PLCC), Spearman Rank Order Correlation Coefficient (SROCC), and Root Mean Squared Error (RMSE) for performance comparison. PLCC reflects the linear correlation between prediction and ground truth, and SROCC measures the rank correlation between objective and subjective scores. RMSE reflects the prediction accuracy. The floating range of the three indices is [0,1]. The closer the values of PLCC and SROCC are to 1, the closer RMSE is to 0, indicating that the prediction result is better. Moreover, we perform a non-linear mapping suggested in [43] when calculating the metrics. The five-parameter logistic function can be described as:

$$f(Q) = \beta_1 \left(\frac{1}{2} - \frac{1}{1 + e^{[\beta_2(Q - \beta_3)]}} \right) + \beta_4 Q + \beta_5, \quad (6)$$

where Q is the prediction score and $f(Q)$ is the corresponding mapped objective quality score. The $\beta_1, \beta_2, \dots, \beta_5$ are parameters to be fitted by minimizing the sum of squared errors between the mapped objective score $f(Q)$ and the ground truth.

C. Network Training

For data pre-processing, we crop raw distorted stereo pairs in four databases to non-overlapping 40×40 patches to solve the data deficiency problem. We assign the subjective score of source images as the label of corresponding patch pairs and feed 64 patches per mini-batch to the model. PyTorch is used for implementation on an NVIDIA TITAN X Pascal GPU with 12GB memory. We utilize the Adam [44] optimizer with the default momentum values of (0.9, 0.999) for (β_1 and β_2). The weight decay is set to 0.0004. The initial learning rate is 1×10^{-4} , and we adopt cosine decay with warm restarts [45] to adjust it for 100 epochs. We randomly divide 80% of the distorted image pairs as the training set and the rest 20% as the

TABLE II
PERFORMANCE COMPARISON ON THE TWO LIVE 3D DATABASES.

Methods	LIVE 3D Phase I			LIVE 3D Phase II			
	PLCC	SROCC	RMSE	PLCC	SROCC	RMSE	
Traditional models	Chen [23]	0.895	0.891	7.247	0.880	0.880	5.102
	Zhou2016 [5]	0.928	0.887	6.025	0.861	0.823	5.779
	Yang [24]	0.9364	0.9289	5.2575	0.9131	0.8747	5.0994
	Messai2020 [9]	0.939	0.930	5.605	0.922	0.913	4.352
	Liu [38]	0.958	0.949	5.069	0.935	0.933	4.014
CNN-based models	Zhang [13]	0.947	0.943	5.336	-	-	-
	Fang [14]	0.957	0.946	-	0.946	0.934	-
	Zhou2019 [16]	0.973	0.965	3.682	0.957	0.947	3.270
	Shi [15]	0.963	0.936	4.161	0.961	0.948	2.675
	Yan [18]	0.962	0.950	-	0.946	0.938	-
	Sun [46]	0.951	0.959	4.573	0.938	0.918	3.809
	Bourbia [17]	0.957	0.942	-	0.921	0.915	-
	Zhou2021 [19]	0.9768	0.9678	3.8204	0.9561	0.9577	3.5649
	Shen [26]	0.972	0.962	-	0.953	0.951	-
	Sim [28]	0.9697	0.9622	3.9441	0.9619	0.955	3.0422
	Si [29]	0.9779	0.9656	2.6077	0.9717	0.9529	2.2771
Ours	SAT-SE	0.9772	0.9739	4.0588	0.9635	0.9607	3.0613
	SAT-CBAM	0.9773	0.9746	3.7831	0.9638	0.9641	2.9126
	SAT-GC	0.9772	0.9723	3.8718	0.9637	0.9616	2.8951

TABLE III
PERFORMANCE COMPARISON ON THE TWO WIVC 3D DATABASES.

Methods	WIVC 3D Phase I			WIVC 3D Phase II		
	PLCC	SROCC	RMSE	PLCC	SROCC	RMSE
Fang [7]	0.953	0.950	-	0.936	0.922	-
Yang [47]	0.9439	0.9246	-	0.9331	0.9143	-
Liu [38]	0.945	0.928	5.268	0.913	0.901	7.658
Sun [46]	-	-	-	0.840	0.835	-
Messai2022 [27]	0.972	0.967	3.635	0.971	0.966	4.161
Sim [28]	0.9625	0.9566	4.1916	0.9698	0.9699	4.5981
Si [29]	0.9690	0.9599	2.9508	0.9580	0.9501	3.0506
SAT-SE	0.9725	0.9698	3.3265	0.9717	0.9705	3.5363
SAT-CBAM	0.9738	0.9740	3.3106	0.9735	0.9734	3.5136
SAT-GC	0.9734	0.9716	3.3051	0.9732	0.9718	3.5260

testing set for each database. The k-fold cross-validation ($k = 10$ in our experiments) is carried out over four datasets and the mean value is adopted. The Euclidean distance is applied to the training process. The loss function can be formulated as:

$$\text{Loss} = \frac{1}{N} \sum_{n=1}^N \|f(x_n; \omega) - y_n\|_2^2, \quad (7)$$

where N is the number of training patch pairs in a batch, $f(x_n; \omega)$ is the predicted quality score of the n -th input pairs x_n , and y_n is the corresponding ground truth.

D. Performance comparison

We reconstruct three well-known attention blocks with SAT structure for NR-SIQA, including SE [30], CBAM [31], and GC [33]. We stack 7 SAT blocks ($n = 7$) for these three variants for overall performance comparison. We compare our models with sixteen state-of-the-art NR-SIQA methods on LIVE 3D databases, including five traditional [5], [9], [23], [24], [38] and eleven CNN-based methods [13]–[19], [26], [28], [29], [46]. Seven state-of-the-art NR-SIQA methods

are compared with our networks on WIVC 3D databases, including three traditional [7], [38], [47] and four CNN-based methods [27]–[29], [46]. Table II and Table III demonstrate the comparison results on LIVE 3D databases and WIVC 3D databases respectively. The results of all comparison methods are directly borrowed from corresponding papers. And the top three performances are marked as **bold** and unavailable indicators are marked as “-”.

As shown in Table II and Table III, three SATNet variants outperform conventional NR-SIQA methods and obtain competitive indicators against recent-year CNN-based works. SAT-CBAM obtains the best overall performance on four databases due to its rational attention considerations on both channel and spatial dimensions. Generally, most of the traditional works are inferior to CNN-based ones, which can be attributed to the limitations of hand-crafted features and bottom-up design perspective. As a pioneer work of applying CNN to NR-SIQA, Zhang [13] made a great breakthrough compared with other traditional approaches in 2016. Zhou2019 [16] is a classic dual-stream fashion method and its design has got strong performance compared to some research today. Even though Zhou2019 [16] gained better RMSE than our models, SATNets have more powerful performance in terms of three indicators on the LIVE 3D Phase II database, showcasing that simple multi-level binocular interaction mode has a problem in tackling asymmetric distortion. Especially, SATNets lead to a considerable improvement in the LIVE 3D Phase II database, WIVC 3D Phase I, and WIVC 3D Phase II database, indicating the validity of top-down style interactions between binocular and monocular features in processing asymmetric distortion.

Table II and Table III also reveal that StereoIF-Net recently proposed by Si et al. [29] gets the highest PLCC and lowest RMSE in two LIVE 3D databases. This can be credited to the complex structure of StereoIF-Net, in pursuit of simulating both binocular interaction and fusion mechanisms of the

TABLE IV
PLCC COMPARISON OF INDIVIDUAL DISTORTION TYPES ON TWO LIVE 3D DATABASES.

Methods	LIVE 3D Phase I					LIVE 3D Phase II				
	BLUR	FF	JP2K	JPEG	WN	BLUR	FF	JP2K	JPEG	WN
Chen [23]	0.917	0.735	0.907	0.695	0.917	0.941	0.932	0.899	0.901	0.947
Messai2020 [9]	0.935	0.845	0.926	0.668	0.941	0.978	0.925	0.835	0.859	0.953
Liu [38]	0.956	0.855	0.938	0.810	0.966	0.987	0.959	0.936	0.867	0.969
Zhang [13]	0.930	0.883	0.926	0.740	0.944	-	-	-	-	-
Fang [14]	0.953	0.868	0.975	0.753	0.973	0.983	0.929	0.975	0.952	0.972
Zhou2019 [16]	0.974	0.965	0.988	0.916	0.988	0.955	0.994	0.905	0.933	0.972
Sun [46]	0.960	0.890	0.948	0.806	0.956	0.996	0.901	0.900	0.823	0.956
Bourbia [17]	0.972	0.838	0.951	0.744	0.966	0.986	0.948	0.912	0.874	0.924
Zhou2021 [19]	0.9885	0.9315	0.9601	0.9154	0.9796	0.9745	0.9601	0.9221	0.8968	0.9432
Shen [26]	0.988	0.939	0.984	0.906	0.947	0.988	0.964	0.956	0.825	0.954
SAT-SE	0.9956	0.9583	0.9645	0.9346	0.9959	0.9970	0.9605	0.9363	0.9066	0.9992

TABLE V
SROCC COMPARISON OF INDIVIDUAL DISTORTION TYPES ON TWO LIVE 3D DATABASES.

Methods	LIVE 3D Phase I					LIVE 3D Phase II				
	BLUR	FF	JP2K	JPEG	WN	BLUR	FF	JP2K	JPEG	WN
Chen [23]	0.878	0.652	0.863	0.617	0.919	0.900	0.933	0.867	0.867	0.950
Messai2020 [9]	0.887	0.777	0.899	0.625	0.941	0.913	0.925	0.842	0.837	0.943
Liu [38]	0.917	0.821	0.888	0.785	0.951	0.936	0.938	0.909	0.825	0.946
Zhang [13]	0.909	0.834	0.931	0.693	0.946	-	-	-	-	-
Fang [14]	-	-	-	-	-	-	-	-	-	-
Zhou2019 [16]	0.855	0.917	0.961	0.912	0.965	0.600	0.951	0.874	0.747	0.942
Sun [46]	0.979	0.853	0.970	0.687	0.893	0.964	0.918	0.897	0.579	0.933
Bourbia [17]	0.867	0.782	0.908	0.679	0.949	0.924	0.933	0.915	0.874	0.889
Zhou2021 [19]	0.9790	0.9412	0.9429	0.9385	0.9824	0.9333	0.9650	0.9414	0.8681	0.9587
Shen [26]	0.945	0.900	0.965	0.879	0.921	0.951	0.969	0.954	0.816	0.923
SAT-SE	0.9944	0.9097	0.9514	0.9243	0.9965	0.9797	0.9585	0.9423	0.8740	0.9839

HVS. Whereas, huge kernel numbers of convolutional layers are introduced to the intricate binocular interaction module (BIM). High complexity and computational overhead pay for high performance, which will be discussed in more detail in Section IV-G. In contrast, our models obtain the highest PLCC and SROCC values on two WIVC 3D databases with lightweight model design and computational cost.

We also perform individual distortion type tests on two LIVE 3D databases to evaluate the competence of our method when handling specific distortion types. Table IV and Table V provide the comparison results between some methods and SAT-SE on two LIVE 3D databases for PLCC and SROCC metrics respectively, and the top two performances are **bold**. From Table IV and Table V, it is evident that SAT-SE exhibits remarkable performance in predicting quality for specific types of distortions, particularly in the cases of WN and BLUR, outperforming other methods significantly. This superiority can be attributed to its sensitivity towards distortion types characterized by such distributions.

E. Cross-dataset validation

In order to verify the generalization and robustness of the proposed method, cross-database validation experiments on two LIVE 3D databases and two WIVC 3D databases are carried out respectively. The “Training set/Test set” experimental results are illustrated in Table VI and Table VII, the top two metric values are marked as **bold** and unavailable

TABLE VI
PERFORMANCE COMPARISON OF CROSS-DATASET VALIDATION ON TWO LIVE 3D DATABASES.

Methods	LIVE 3D Phase I/II		LIVE 3D Phase II/I	
	PLCC	SROCC	PLCC	SROCC
Messai2020 [9]	0.832	0.823	0.897	0.887
Liu [38]	0.862	0.832	0.888	0.874
Fang [14]	0.811	0.797	0.899	0.898
Zhou2019 [16]	0.710	-	0.932	-
Shi [15]	-	0.793	-	0.901
Shen [26]	0.848	0.833	0.915	0.921
Sim [28]	0.8041	0.7704	0.9083	0.8964
Si [29]	0.8595	0.7972	0.9184	0.9149
SAT-SE	0.8547	0.8378	0.9204	0.9187

indicators are marked as “-”. For example, “LIVE 3D Phase I/II” indicates that the LIVE 3D Phase I database is taken as the training set, and the LIVE 3D Phase II database is used as the test set.

It can be found that the experimental results of cross-dataset validation are not as good as those in the case that the data of the training and test set come from the same database. Yet, our model still has competitive prediction performance over LIVE 3D databases and WIVC 3D databases against other methods. Although PLCC of Liu [38] and Si [29] on LIVE 3D Phase I/II are slightly better than ours, SROCC of SAT-SE outperforms both methods, as well as on other “Training/Test” patterns. Yang [47] reap the best performance on WIVC 3D

TABLE VII
PERFORMANCE COMPARISON OF CROSS-DATASET VALIDATION ON TWO
WIVC 3D DATABASES.

Methods	WIVC 3D Phase I/II		WIVC 3D Phase III/I	
	PLCC	SROCC	PLCC	SROCC
Yang [47]	0.8421	0.8313	0.8739	0.8687
Liu [38]	0.696	0.627	0.701	0.708
Sim [28]	0.7876	0.7547	0.9139	0.9032
Si [29]	0.7816	0.7502	0.8981	0.8712
SAT-SE	0.8065	0.7808	0.9216	0.9126

Phase I/II, but on WIVC 3D Phase II/I, their work significantly underperformed ours and SAT-SE achieves the top one. It is worth highlighting that in both Table VI and Table VII, SAT-SE occupies the highest number of bold values, which reflects the excellent generality of the proposed algorithm.

For both LIVE 3D databases and WIVC 3D databases, the “Phase II/I” pattern consistently yields superior results compared to the “Phase I/II” pattern, as the complexity of distorted images in Phase II surpasses that of Phase I. In addition, the LIVE 3D Phase II dataset contains both symmetrically and asymmetrically distorted stereo pairs while the LIVE 3D Phase I contains only stereo pairs with symmetric distortions. WIVC 3D Phase II database involves more scenes and distorted images than WIVC 3D Phase I database, i.e., more training data have led to better results with the same data complexity.

F. Ablation Study

The experiments of the ablation study are conducted based on SAT-SE implementation in view of its efficiency. The best performance of each experiment is highlighted in **boldface**.

1) Choice of the model scale of SATNet for NR-SIQA:

As mentioned in Section III-B, we construct our model with different scales with a range of SAT block numbers (K). Here we assign $K = 3, 7, 14, 15$, respectively, corresponding to four scales models (Depth = 11, 19, 33, 50, respectively) to investigate the most cost-effective K for the NR-SIQA task. The performances of different scales of SATNet are shown in Table VIII.

A bottleneck layer can significantly reduce the computational cost when increasing the network depth, which is exactly the reason why the 50-layer model has fewer parameters than the 33-layer model (7.80M versus 8.51M). From experimental results, we observe that with more SAT blocks stacked, SATNet goes deeper and performs better in general. Inevitably, the deep model incurs more redundant parameters, manifesting overfitting and performance degradation on both databases. Notably, even shallower models ($K = 3, 7$) attain the best PLCC, SROCC, and RMSE on LIVE 3D Phase I. Consequently, we choose $K = 7$ for overall experiments in pursuit of the balance between performance improvement and computational overhead.

2) *Verification of top-down philosophy*: In order to verify the inherent superiority of the top-down perspective, a series of comparison experiments of three different model design philosophies are also conducted. The results are reported in

Table IX. As categorized in Section I, there are two classic model structures for NR-SIQA from a bottom-up design perspective: a dual-stream network without any interaction between two monocular branches before the last fusion; a multi-level network where the fusion or difference features are obtained as the interactive information. Accordingly, we remove all SAT blocks to implement the first structure on SATNet and denote it as “Bottom-up-1”. “Bottom-up-2” indicates that fusion and difference maps are obtained after the first, third, fifth, and seventh residual blocks and concatenated before regression based on “Bottom-up-1”. Moreover, we substitute SAT blocks in SATNet with vanilla attention blocks to conduct a comparison experiment, which is also bottom-up and labeled as “Bottom-up-3”. Specifically, two outputs of monocular branches are concatenated and fed into the attention module. Then re-weighted combined features are divided into two monocular views again in the channel dimension and forwarded to their original branches.

It can be found from Table IX that Bottom-up-2 and Bottom-up-3 both improve the performance against Bottom-up-1, signifying the vital influence of binocular interactive properties. The proposed SATNet obtains the best performance among all competitors, which can prove the effectiveness of the top-down design philosophy.

3) *Effects of Energy Coefficient*: We visualize four ECs’ updating processes during training on two databases in Fig. 5. α_i represents the corresponding EC in the i th SAT block. We can observe that the four curves converge quickly and maintain stability in their values individually after about 10 epochs. The same phase’s EC on LIVE 3D Phase I is different from LIVE 3D Phase II, and different phase’s ECs on the same database are also diverse, which reflects that EC can adjust the magnitude of binocular response adaptively. Experimental results show that the introduced EC improves PLCC and SROCC by 0.003 and 0.002 on LIVE 3D Phase I and by 0.003 and 0.005 on LIVE 3D Phase II, respectively, compared without multiplying EC.

4) *Verification of dual-pooling strategy*: To verify the superiority of the proposed dual-pooling strategy, we conduct several comparison experiments by adopting some common pooling manners, e.g., average pooling (AVG), max pooling (Max), and min pooling (Min). Results are revealed in Table XI. “+” and “-” in the table remark fusion and difference maps respectively. For instance, the first row of Table XI denotes that both fusion and difference features are processed by average pooling operation before regression, since both “+” and “-” symbols are in the “Avg” column. We can find that the using of average pooling leads to performance deterioration. Although average pooling excels in integrating contextual information, it will smooth learned sharp quality features and cannot get desirable results. Most works generally operate max pooling on both fusion and difference maps (the second row of Table XI), while it can be seen from the indices that our dual-pooling strategy (the last row of Table XI) can filter crucial distortion information for quality regression and achieve the best performance.

TABLE VIII
PERFORMANCE COMPARISON OF DIFFERENT MODEL SCALES ON TWO LIVE 3D DATABASES.

Block number (K)	Depth (layers)	#Param.	LIVE 3D Phase I			LIVE 3D Phase II		
			PLCC	SROCC	RMSE	PLCC	SROCC	RMSE
$K = 3$	11	6.87M	0.9758	0.9751	3.8932	0.9615	0.9590	2.9347
$K = 7$	19	7.47M	0.9772	0.9739	4.0588	0.9635	0.9607	3.0613
$K = 14$	33	8.51M	0.9741	0.9703	4.5037	0.9644	0.9628	2.9466
$K = 15$	50	7.80M	0.9743	0.9733	4.6435	0.9640	0.9593	2.9388

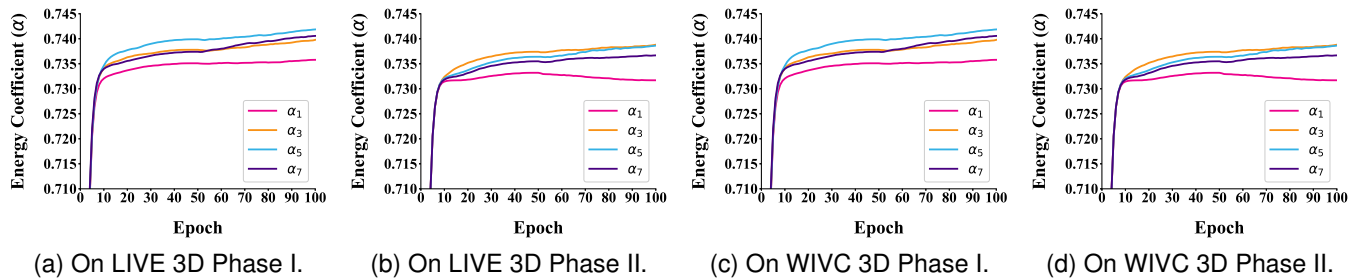


Fig. 5. Learning processes of Energy Coefficients (EC) in SAT-SE in different phases on four 3D databases.

TABLE IX
PERFORMANCE COMPARISON OF DESIGN PERSPECTIVES ON TWO LIVE 3D DATABASES.

Methods	LIVE 3D Phase I		LIVE 3D Phase II	
	PLCC	SROCC	PLCC	SROCC
bottom-up-1	0.9563	0.9401	0.9445	0.9321
bottom-up-2	0.9584	0.9440	0.9564	0.9423
bottom-up-3	0.9625	0.9544	0.9529	0.9420
top-down (SAT-SE)	0.9772	0.9739	0.9635	0.9607

TABLE X
PERFORMANCE COMPARISON OF EC ON TWO LIVE 3D DATABASES.

Methods	LIVE 3D Phase I		LIVE 3D Phase II	
	PLCC	SROCC	PLCC	SROCC
without EC	0.9592	0.9531	0.9489	0.9465
SAT-SE	0.9772	0.9739	0.9635	0.9607

G. Computational Complexity

From the perspective of network structure design, the previous work StereoIFNet is obviously more complex than SATNet.

V. CONCLUSION

In conclusion, our work contributes to the field of stereoscopic image quality assessment by introducing a top-down approach via stereo attention. The proposed stereo attention network, SAT block, and dual-pooling strategy collectively provide a comprehensive framework for assessing the quality of stereoscopic images.

The introduced learnable Energy Coefficient can dynamically adjust the magnitude of binocular response. Experimental results prove the philosophy and superiority of our SATNet. Furthermore, we will explore more possibilities.

TABLE XI
PERFORMANCE COMPARISON OF DIFFERENT POOLING STRATEGIES ON THE LIVE 3D PHASE II DATABASE.

Pooling strategies			PLCC	SROCC
Avg	Max	Min		
+-			0.9465	0.9421
	+-		0.9588	0.9579
		+-	0.9503	0.9487
	+	-	0.9576	0.9543
	-	+	0.9635	0.9607

TABLE XII
COMPUTATIONAL COMPLEXITY COMPARISON ON THE LIVE 3D PHASE I DATABASE.

Methods	#Param.	Inference time (sec)
Fang [14]	0	0
Shen [26]	0	0
Zhou [16]	0	0
Si [29]	0	0
SAT-SE	7.47M	0
SAT-CBAM	0	0
SAT-GC	0	0

REFERENCES

- [1] M.-J. Chen, C.-C. Su, D.-K. Kwon, L. K. Cormack, and A. C. Bovik, "Full-reference quality assessment of stereopairs accounting for rivalry," *Signal Processing: Image Communication*, vol. 28, no. 9, pp. 1143–1155, 2013.
- [2] Z. Wang, E. Simoncelli, and A. Bovik, "Multiscale structural similarity for image quality assessment," in *The Thirty-Seventh Asilomar Conference on Signals, Systems & Computers, 2003*, vol. 2, 2003, pp. 1398–1402 Vol.2.
- [3] N. Kruger, P. Janssen, S. Kalkan, M. Lappe, A. Leonardis, J. Piater, A. J. Rodriguez-Sanchez, and L. Wiskott, "Deep hierarchies in the primate visual cortex: What can we learn for computer vision?" *IEEE Transactions on Pattern Analysis and Machine Intelligence*, vol. 35, no. 8, pp. 1847–1871, 2013.
- [4] B. Shi, T. Darrell, and X. Wang, "Top-down visual attention from analysis by synthesis," 2023.

- [5] W. Zhou and L. Yu, "Binocular responses for no-reference 3d image quality assessment," *IEEE Transactions on Multimedia*, vol. 18, no. 6, pp. 1077–1084, 2016.
- [6] W. Zhou, L. Yu, Y. Zhou, W. Qiu, M.-W. Wu, and T. Luo, "Blind quality estimator for 3d images based on binocular combination and extreme learning machine," *Pattern Recognition*, vol. 71, pp. 207–217, 2017.
- [7] Y. Fang, J. Yan, J. Wang, X. Liu, G. Zhai, and P. Le Callet, "Learning a no-reference quality predictor of stereoscopic images by visual binocular properties," *IEEE Access*, vol. 7, pp. 132 649–132 661, 2019.
- [8] Y. Liu, W. Yan, Z. Zheng, B. Huang, and H. Yu, "Blind stereoscopic image quality assessment accounting for human monocular visual properties and binocular interactions," *IEEE Access*, vol. 8, pp. 33 666–33 678, 2020.
- [9] O. Messai, F. Hachouf, and Z. A. Seghir, "Adaboost neural network and cyclopean view for no-reference stereoscopic image quality assessment," *Signal Processing: Image Communication*, vol. 82, p. 115772, 2020.
- [10] A. Krizhevsky, I. Sutskever, and G. E. Hinton, "Imagenet classification with deep convolutional neural networks," *Commun. ACM*, vol. 60, no. 6, p. 84–90, may 2017.
- [11] J. Long, E. Shelhamer, and T. Darrell, "Fully convolutional networks for semantic segmentation," in *2015 IEEE Conference on Computer Vision and Pattern Recognition (CVPR)*, 2015, pp. 3431–3440.
- [12] S. Ren, K. He, R. Girshick, and J. Sun, "Faster r-cnn: Towards real-time object detection with region proposal networks," in *Advances in Neural Information Processing Systems 28 (NIPS 2015)*, ser. Advances in Neural Information Processing Systems, vol. 28, 2015.
- [13] W. Zhang, C. Qu, L. Ma, J. Guan, and R. Huang, "Learning structure of stereoscopic image for no-reference quality assessment with convolutional neural network," *Pattern Recognition*, vol. 59, pp. 176–187, 2016.
- [14] Y. Fang, J. Yan, X. Liu, and J. Wang, "Stereoscopic image quality assessment by deep convolutional neural network," *Journal of Visual Communication and Image Representation*, vol. 58, pp. 400–406, 2019.
- [15] Y. Shi, W. Guo, Y. Niu, and J. Zhan, "No-reference stereoscopic image quality assessment using a multi-task cnn and registered distortion representation," *Pattern Recognition*, vol. 100, p. 107168, 2020.
- [16] W. Zhou, Z. Chen, and W. Li, "Dual-stream interactive networks for no-reference stereoscopic image quality assessment," *IEEE Transactions on Image Processing*, vol. 28, no. 8, pp. 3946–3958, 2019.
- [17] S. Bourbia, A. Karine, A. Chetouani, and M. E. Hassoun, "A multi-task convolutional neural network for blind stereoscopic image quality assessment using naturalness analysis," in *2021 IEEE International Conference on Image Processing (ICIP)*, 2021, pp. 1434–1438.
- [18] J. Yan, Y. Fang, L. Huang, X. Min, Y. Yao, and G. Zhai, "Blind stereoscopic image quality assessment by deep neural network of multi-level feature fusion," in *2020 IEEE International Conference on Multimedia and Expo (ICME)*, 2020, pp. 1–6.
- [19] M. Zhou and S. Li, "Deformable convolution based no-reference stereoscopic image quality assessment considering visual feedback mechanism," in *2021 International Conference on Visual Communications and Image Processing (VCIP)*, 2021, pp. 01–05.
- [20] S. Li, P. Zhao, and Y. Chang, "No-reference stereoscopic image quality assessment based on visual attention mechanism," in *2020 IEEE International Conference on Visual Communications and Image Processing (VCIP)*, 2020, pp. 326–329.
- [21] B. Mitchell, K. Dougherty, J. Westerberg, B. Carlson, L. Daumail, A. Maier, and M. Cox, "Stimulating both eyes with matching stimuli enhances v1 responses," *iScience*, vol. 25, p. 104182, 04 2022.
- [22] S.-H. Zhang, X. Zhao, S.-M. Tang, and C. Yu, "Neuronal responses to monocular and binocular stimulations in macaque v1 studied with two-photon calcium imaging," 09 2022. [Online]. Available: https://www.researchgate.net/publication/363631428_Neuronal_responses_to_monocular_and_binocular_stimulations_in_macaque_V1_studied_with_two-photon_calcium_imaging
- [23] M.-J. Chen, L. K. Cormack, and A. C. Bovik, "No-reference quality assessment of natural stereopairs," *IEEE Transactions on Image Processing*, vol. 22, no. 9, pp. 3379–3391, 2013.
- [24] J. Yang, B. Jiang, H. Song, X. Yang, W. Lu, and H. Liu, "No-reference stereoimage quality assessment for multimedia analysis towards internet-of-things," *IEEE Access*, vol. 6, pp. 7631–7640, 2018.
- [25] J. Yang, Y. Zhao, Y. Zhu, H. Xu, W. Lu, and Q. Meng, "Blind assessment for stereo images considering binocular characteristics and deep perception map based on deep belief network," *Information Sciences*, vol. 474, pp. 1–17, 2019.
- [26] L. Shen, X. Chen, Z. Pan, K. Fan, F. Li, and J. Lei, "No-reference stereoscopic image quality assessment based on global and local content characteristics," *Neurocomputing*, vol. 424, pp. 132–142, 2021.
- [27] O. Messai and A. Chetouani, "End-to-end deep multi-score model for no-reference stereoscopic image quality assessment," in *2022 IEEE International Conference on Image Processing (ICIP)*, 2022, pp. 2721–2725.
- [28] K. Sim, J. Yang, W. Lu, and X. Gao, "Blind stereoscopic image quality evaluator based on binocular semantic and quality channels," *IEEE Transactions on Multimedia*, vol. 24, pp. 1389–1398, 2022.
- [29] J. Si, B. Huang, H. Yang, W. Lin, and Z. Pan, "A no-reference stereoscopic image quality assessment network based on binocular interaction and fusion mechanisms," *IEEE Transactions on Image Processing*, vol. 31, pp. 3066–3080, 2022.
- [30] J. Hu, L. Shen, and G. Sun, "Squeeze-and-excitation networks," in *2018 IEEE/CVF Conference on Computer Vision and Pattern Recognition*, 2018, pp. 7132–7141.
- [31] S. Woo, J. Park, J.-Y. Lee, and I. S. Kweon, "Cbam: Convolutional block attention module," in *Computer Vision – ECCV 2018*, V. Ferrari, M. Hebert, C. Sminchisescu, and Y. Weiss, Eds. Cham: Springer International Publishing, 2018, pp. 3–19.
- [32] X. Wang, R. Girshick, A. Gupta, and K. He, "Non-local neural networks," in *2018 IEEE/CVF Conference on Computer Vision and Pattern Recognition*, 2018, pp. 7794–7803.
- [33] Y. Cao, J. Xu, S. Lin, F. Wei, and H. Hu, "Gcnet: Non-local networks meet squeeze-excitation networks and beyond," in *2019 IEEE/CVF International Conference on Computer Vision Workshop (ICCVW)*, 2019, pp. 1971–1980.
- [34] X. Li, W. Wang, X. Hu, and J. Yang, "Selective kernel networks," in *2019 IEEE/CVF Conference on Computer Vision and Pattern Recognition (CVPR)*, 2019, pp. 510–519.
- [35] K. He, X. Zhang, S. Ren, and J. Sun, "Deep residual learning for image recognition," in *2016 IEEE Conference on Computer Vision and Pattern Recognition (CVPR)*, 2016, pp. 770–778.
- [36] —, "Identity mappings in deep residual networks," in *Computer Vision – ECCV 2016*, B. Leibe, J. Matas, N. Sebe, and M. Welling, Eds. Cham: Springer International Publishing, 2016, pp. 630–645.
- [37] X. Ma, J. Guo, S. Tang, Z. Qiao, Q. Chen, Q. Yang, S. Fu, P. Palacharla, N. Wang, and X. Wang, "Learning connected attentions for convolutional neural networks," in *2021 IEEE International Conference on Multimedia and Expo (ICME)*, 2021, pp. 1–6.
- [38] Y. Liu, C. Tang, Z. Zheng, and L. Lin, "No-reference stereoscopic image quality evaluator with segmented monocular features and perceptual binocular features," *Neurocomputing*, vol. 405, pp. 126–137, 2020.
- [39] G. E. Hinton, N. Srivastava, A. Krizhevsky, I. Sutskever, and R. R. Salakhutdinov, "Improving neural networks by preventing co-adaptation of feature detectors," 2012.
- [40] A. K. Moorthy, C.-C. Su, A. Mittal, and A. C. Bovik, "Subjective evaluation of stereoscopic image quality," *Signal Processing: Image Communication*, vol. 28, no. 8, pp. 870–883, 2013.
- [41] J. Wang and W. Zhou, "Perceptual quality of asymmetrically distorted stereoscopic images: The role of image distortion types," in *International Workshop on Video Processing & Quality Metrics for Consumer Electronics*, 2014.
- [42] J. Wang, A. Rehman, K. Zeng, S. Wang, and Z. Wang, "Quality prediction of asymmetrically distorted stereoscopic 3d images," *IEEE Transactions on Image Processing*, vol. 24, no. 11, pp. 3400–3414, 2015.
- [43] H. Sheikh, M. Sabir, and A. Bovik, "A statistical evaluation of recent full reference image quality assessment algorithms," *IEEE Transactions on Image Processing*, vol. 15, no. 11, pp. 3440–3451, 2006.
- [44] D. P. Kingma and J. Ba, "Adam: A method for stochastic optimization," in *ICLR (Poster)*, 2015. [Online]. Available: <http://arxiv.org/abs/1412.6980>
- [45] I. Loshchilov and F. Hutter, "SGDR: Stochastic gradient descent with warm restarts," in *International Conference on Learning Representations*, 2017. [Online]. Available: <https://openreview.net/forum?id=Skq89Scxx>
- [46] G. Sun, B. Shi, X. Chen, A. S. Krylov, and Y. Ding, "Learning local quality-aware structures of salient regions for stereoscopic images via deep neural networks," *IEEE Transactions on Multimedia*, vol. 22, no. 11, pp. 2938–2949, 2020.
- [47] J. Yang, K. Sim, X. Gao, W. Lu, Q. Meng, and B. Li, "A blind stereoscopic image quality evaluator with segmented stacked autoencoders considering the whole visual perception route," *IEEE Transactions on Image Processing*, vol. 28, no. 3, pp. 1314–1328, 2019.



Huilin Zhang received his Bachelor's degree from Tianjin University, Tianjin, China in 2021. He is currently pursuing a Master's degree at the School of Electrical and Information Engineering, Tianjin University. His research interests include 3D image processing and quality evaluation, attention mechanisms, neural networks, and deep learning.



Sumei Li received the Ph.D. from Nankai University, Tianjin, China. Since 2006, she has been an Associate Professor with the Communication Engineering Department, Tianjin University. She chaired a national 863 project, a National Natural Science Foundation, and a key fund in Tianjin. Her research interests include 3D image/video transmission, processing and quality evaluation, depth/image SR reconstruction, sparse representation, neural networks, and deep learning. Dr. Li is a member of China's neural network committee.



Yongli Chang has studied for a Ph.D. degree in the School of Electrical and Information Engineering at Tianjin University since 2019. She received her Master's degree in the School of Electrical and Information Engineering at Tianjin University in 2019. Her research interests include 2D/3D image quality evaluation, neural networks, deep learning, and signal sparse representation.